Article Title: Fibrin-modulating nanogels for treatment of disseminated intravascular coagulation

Short Title: Fibrin nanogels to treat DIC

Emily P. Mihalko[1,2]; Megan Sandry[1], Nicholas Mininni[1], Kimberly Nellenbach[1,2], Halston Deal[1,2], Michael Daniele[1,2,3], Kamrouz Ghadimi [4], Jerrold H. Levy[4], Ashley C. Brown[1,2]

[1]Joint Department of Biomedical Engineering of University of North Carolina – Chapel Hill and North Carolina State University, Raleigh, NC 27695

[2]Comparative Medicine Institute, North Carolina State University, Raleigh, NC 27606

[3]Department of Electrical and Computer Engineering, North Carolina State University, Raleigh, NC 27695

[4]Duke University School of Medicine, Department of Anesthesiology and Critical Care, Durham, NC

*Corresponding Author: Ashley C. Brown, PhD
Address: Joint Department of Biomedical Engineering
North Carolina State University and University of North Carolina at Chapel-Hill
1001 William Moore Dr., Raleigh, NC, 27606
Phone: (919) 513-8231
Email: aecarso2@ncsu.edu

Text word count: 5157
Abstract word count: 200
Number of figures and tables: 6
Number of references: 57
Scientific category: Thrombosis and Hemostasis

Key Points

- Fibrin targeting nanogels promote maturation of actively polymerizing clots; when loaded with tissue-type plasminogen activator they lyse clots.
- Loaded nanogels can treat microthrombi formation and bleeding complications associated with disseminated intravascular coagulation.

Visual Abstract

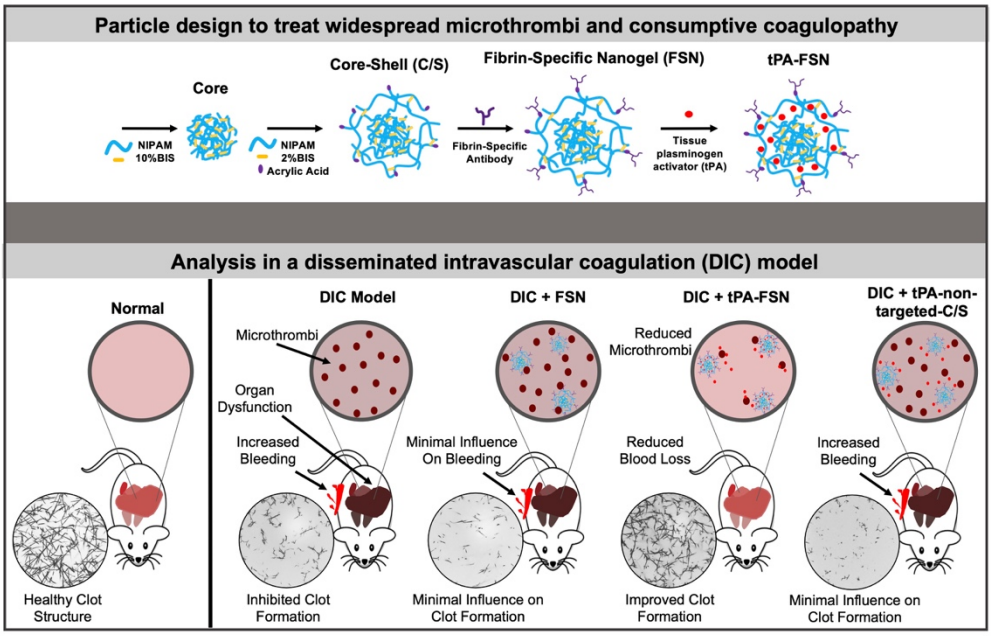

Abstract

Disseminated intravascular coagulation (DIC) is a pathological coagulopathy associated with infection that increases mortality. In DIC, excessive thrombin generation causes microthrombi formation to multiorgan failure; bleeding risks can also be a concern due to clotting factor consumption. Different clinical events lead to DIC including sepsis, trauma, and shock. Treatment for either thrombotic or bleeding presentation in DIC is opposing, creating therapeutic dilemmas in management. The objective of this study was to develop fibrin-specific core-shell

nanogels (FSNs) loaded with tissue-type plasminogen activator (tPA) to treat the microcirculatory complications of DIC, facilitating targeted clot dissolution to manage microthrombi, and the potential consumptive coagulopathy causing bleeding. FSNs enhance formation of actively polymerizing clots by crosslinking fibrin fibers but can also target pre-existing microthrombi, and when loaded with tPA, facilitate targeted delivery to lyse the microthrombi. We hypothesized that this dual action would simultaneously address bleeding and microthrombi with DIC to improve outcomes. *In vivo*, tPA-FSNs decreased multiorgan microthrombi presentation, recovered platelet counts, and improved bleeding outcomes in a DIC rodent model. When incorporated with human DIC patient plasma, tPA-FSNs restored clot structure and clot growth under flow. Together, these data demonstrate that a fibrinolytic agent loaded into fibrin-targeting nanogels could improve DIC outcomes.

Introduction

Disseminated intravascular coagulation (DIC) is a condition characterized by pathological coagulopathy. It is associated with up to 19% of intensive care unit admissions and has a high mortality rate of 40-78% depending on diagnostic criteria[1–4]. Various clinical events can lead to DIC including infection, trauma, cancer, pregnancy, and liver disease[5–11]. DIC may occur in 30-50% of cases of severe sepsis, a leading cause of death worldwide[12–14], and also in critically ill patients with COVID-19 due to secondary infections[8–11]. Due to the high mortality associated with DIC, novel therapies are critically needed to improve outcomes.

DIC is a complex, acquired coagulopathy that is characterized by uncontrolled thrombin generation throughout the intravascular system[15,16]. As thrombin is generated, fibrin deposits in the microvasculature, leading to ischemic tissue damage and multi-organ failure. As part of this complex response, microthrombi consume clotting factors and can subsequently initiate

fibrinolytic pathways that in turn, lead to diffuse bleeding[15,17]. Current treatment for DIC mainly involves treatment of the underlying condition, but in circumstances of severe thrombosis or severe bleeding, thrombolytic therapies or procoagulants, platelets or plasma transfusions respectively may be administered[7,14,18,19]. However, because simultaneous thrombosis and bleeding can occur in DIC, and treatment strategies for either presentation are opposing, controlling the hemostatic imbalance can be elusive, resulting in the significant mortality rate of the disorder.

The coagulation cascade culminates in the formation of fibrin through the polymerization of fibrinogen that is initiated by the serine protease thrombin, forming an insoluble matrix[20]. The dynamics of fibrin polymerization therefore play a central role in thrombosis and bleeding as thrombosis due to fibrin formation in the microcirculation, as in DIC, decreases blood flow causing tissue damage, while deficient fibrin polymerization is critical during hemostasis in preventing exsanguination[21–25]. Methods to regulate the dynamics of fibrin polymerization include the inhibition of coagulation activation, such as antithrombin, protein C, or tissue factor pathway inhibitor, most of which have been studied for treating thromboinflammatory diseases such as DIC[26,27]. Additionally, the fibrinolytic system regulates fibrin dynamics by the lysis of pre-formed clots containing fibrin through plasmin activation[28]. Tissue-type plasminogen activator (tPA) is a major initiator of fibrinolytic pathways as it catalyzes the conversion of plasminogen into plasmin to lyse clots[29]. In DIC, deranged fibrin polymerization occurs for thrombi formation, along with a consumptive coagulopathy with inadequate substrates necessary for clot formation thereby leading to bleeding complications.

In developing therapeutics for thrombotic and/or hemostatic complications, targeting fibrin is a promising strategy. However, with current treatment strategies for thrombosis and bleeding, off-target effects with systemic agents can easily alter the hemostatic balance at non-injured sites[30].

Therefore, in treating a disorder such as DIC where the coagulation imbalance occurs systemically, targeting a coagulation protein such as fibrin could help regulate excessive thrombi formation and bleeding risks. We hypothesize that simultaneously addressing bleeding and microthrombi associated with DIC will improve clinical outcomes. In this study, novel fibrin-specific nanogels (FSN) have been developed using nanoscale colloidal hydrogels coupled to a fibrin-specific antibody, and loaded with a fibrinolytic agent, tPA, to create a novel therapeutic that balances the procoagulant and fibrinolytic shutdown that occurs in DIC (Figure 1). Unloaded FSNs target the clotting process by crosslinking fibrin fibers and assist in maturation of actively polymerizing clots, while tPA-loaded nanogels facilitate directed lysis of aberrant thrombi formed in DIC (Figure 1A). The overall objective in this study was to examine the ability for fibrin-targeting core-shell nanogels to modulate overall fibrin dynamics in DIC by promoting lysis of pre-existing clots and promoting clotting abilities at sites of injury in order to restore the overall hemostatic balance. We demonstrate *in vivo* in a rodent model of DIC and *in vitro* in DIC patient plasma samples that fibrin-targeting nanogels delivering tPA can treat aberrant clot formation to restore coagulation potential and mitigate DIC complications of thrombosis and bleeding to improve outcomes.

Methods.

Nanogel synthesis and characterization

Core-shell poly(N-isopropylacrylamide) p(NIPAM) nanogels were synthesized in two precipitation polymerization reactions[31]. Cores containing 90% N-isopropylacrylamide (NIPAM) and 10% N,N'-methylenebis(acrylamide) (BIS) (Sigma-Aldrich); shells containing 93% NIPAM, 2% BIS, and 5% acrylic acid (AAc) were synthesized around cores. AAc dispersed throughout the nanogel shell acts as chemoligation sites for subsequent antibody conjugation. Nanogels were

filtered through glass wool and purified via dialysis. 0.1% methacryloxyethyl thiocarbamoyl rhodamine B monomer (Poly-science) was incorporated for fluorescence. For biodistribution studies, FSNs were conjugated to VivoTag-S 750 Fluorochrome (PerkimElmer). Single-layer nanogels were synthesized containing 93% NIPAM, 2% BIS, and 5% AAc. Size and morphological characterization included particle tracking analysis (Malvern Nanosight), atomic force microscopy (AFM), and scanning electron microscopy (SEM). FSNs and control particles were made by conjugating either a sheep antihuman fibrin fragment E polyclonal antibody (Affinity Biologicals) or a sheep IgG isotype control (ThermoFisher) respectively to core-shell particles utilizing EDC/Sulfo-NHS chemistry. From a known particle/mL concentration found through Nanosight particle tracking, the amount of fragment E antibody or control sheep IgG was determined using a CBQCA Protein Quantitation Kit (ThermoFisher) conducted in duplicate for three particle suspensions.

Nanogel drug-loading and release characterization

Lyophilized particles were resuspended at high concentrations (20mg/mL) in loading solutions of 29 μg/mL tPA (Sigma Aldrich) to load through a rehydration technique, which allows for drug entanglement within the polymer network of the nanogels upon nanogel swelling in solution[32,33]. After agitation for 24 hours, particles were centrifuged, washed, and resuspended in HEPES buffer (25 mM HEPES, 0.15 M NaCl, 5 mM $CaCl_2$, pH 7.4). At various time points (1-168 hours) the particles were centrifuged, and release supernatant was collected. Detection of released material was determined through fluorescence scans (for drug mimics) or tPA ELISA (ab190812). Three separate samples for each condition were examined.

To examine potential aggregation of particles, FSNs and tPA-FSNs were added to platelet poor plasma (NYBC), whole blood obtained in sodium citrate from LPS-induced DIC rats, and

whole blood with the addition of 10% rat complement serum (ab155157 Abcam). A final 2mg/mL concentration of particles was added to plasma or whole blood samples with 25μg/mL anti-sheep FITC secondary antibody (FisherScientific), 5mM $CaCl_2$, 0.1mg/mL AlexaFluor 594 conjugate fibrinogen (FisherScientifc), and 0.5U/mL thrombin. After 2 hours, confocal microscopy was used to visualize the particles.

Clotting analysis with tPA-loaded fibrin-specific nanogels under static and fluidic conditions under active coagulation

tPA (29 μg/mL) was loaded into purified FSNs or CS-IgGs (tPA-FSNs and tPA-CS-IgG respectively). After separating loading solution, washing, and lyophilizing, particles were incorporated into an endogenous fibrinolysis absorbance-based clotting assay for static clotting analysis[34]. To test clotting dynamics under fluidic conditions, a custom T-junction polydimethylsiloxane (PDMS) fluidic device was used. A stationary fibrin clot boundary was formed at the T-junction and actively polymerizing solutions flowed into the device. Treatment conditions in the flow solution included buffer, FSNs, non-binding core-shell nanogels (C/S), tPA-FSNs, tPA loaded into non-binding core-shell nanogels (tPA-C/S), tPA alone, and tPA-CS-IgGs. tPA alone doses were previously established from studies using the same nanogel formulation[31]. A negative control of FSNs under non-polymerizing conditions was also conducted. For 20 minutes, images were taken and the distance between clot apexes measured.

To examine how unloaded FSNs enhance fibrin polymerization, confocal microscopy was utilized to examine fibrin clot structure. Clots were made by adding 0.25 U/mL human alpha-thrombin (Fisher Scientific) and 0.05 mg/mL Alexa-Fluor 488 labeled fibrinogen (ThermoFisher) to 2mg/mL fibrinogen (FIB3, Enzyme Research Laboratories) in HEPES buffer with 1mg/mL

FSNs or CS-IgG control particles. Fiber density was quantified from three z-stacks per clot and three separate clots were analyzed.

In vivo evaluation of tPA-FSN treatment and biodistribution in a rodent model of DIC

In vivo experimentation was approved by North Carolina State University Institutional Animal Care and Use Committee and conducted in AAALAC international-accredited facilities. Adult male Sprague Dawley rats received intravenous infusion of 30 mg/kg lipopolysaccharide (LPS) over 4 hours to induce DIC[35,36]. Saline, FSNs, tPA-FSNs, or tPA-CS-IgGs (10mg/kg) were then injected via tail vein and circulated for 30 minutes. Terminal blood draws were performed to evaluate coagulation parameters and organs were harvested to evaluate thrombus formations. Control animals did not receive LPS or treatment. Martius-scarlet-blue (MSB) staining and immunohistochemistry (IHC) with anti-fibrin antibody (UC45) (GeneTex) were performed for fibrin microthrombi visualization. Quantification of fibrin microthrombi was conducted from fibrin IHC tissue sections. Three tissue sections from the heart, lung, kidney, and liver from each animal were imaged using EVOS FL Auto Imaging System. A particle count for microthrombi was obtained using ImageJ particle analysis software. Average fibrin particle counts for each organ for each animal are shown.

Manual platelet counts were conducted using a hemocytometer and platelet poor plasma (PPP) was isolated from whole blood collected in sodium citrate for each animal. Fibrinogen and D-Dimer ELISAs were performed (Abcam, MyBiosource). Confocal and cryogenic SEM (cryoSEM) were utilized to examine *ex vivo* fibrin clot structure of PPP from control and DIC animals in order to further examine clotting factor consumption of DIC. For confocal microscopy, plasma was polymerized by adding 0.5 U/mL human alpha-thrombin (Fisher Scientific) with 5mM $CaCl_2$ and 0.05 mg/mL Alexa-Fluor 488 labeled fibrinogen (ThermoFisher) for visualization. *Ex*

vivo clots polymerized for two hours prior to imaging. Fiber density was quantified from three z-stacks per clot. For cryoSEM, clots were made from PPP and 0.5 U/mL thrombin and were imaged three hours after polymerization.

To determine potential effects of circulating particles left in the plasma, a dot blot was performed on the plasma samples to detect particles. Rabbit anti-sheep IgG (ThermoFisher 31627) was used as a primary antibody and IRDye 800CW goat anti-rabbit IgG secondary antibody was used for detection on a Licor Odyssey CLx Imaging system where subsequent analysis was conducted. Additionally, 1mg/mL FSNs or tPA-FSNs was exogenously added to PPP clots made from DIC animals treated with saline. Clots were polymerized and imaged as described above with 1U/mL thrombin. Fiber density was quantified as previously described to evaluate clot structure.

Biodistribution of tPA-FSNs and FSNs in DIC animals was conducted by injecting 10 mg/kg particles or saline following DIC induction with LPS as described above. After 30 min, animals were sacrificed and organs, blood, and urine collected. An IVIS Xenogen In Vivo Imager was utilized to scan organs *ex vivo* and evaluate the presence of particles in the heart, lung, liver, kidney, and spleen. A dot blot was performed on the urine and whole blood samples as described above.

In vivo evaluation of bleeding in a rodent model of DIC with tPA-FSN treatment

The LPS-DIC model was utilized and after 30 minutes of treatment (saline, FSNs, tPA-FSNs, or tPA-CS-IgGs) a liver laceration injury was conducted[37]. Separate cohorts of animals acted as a control or vehicle condition. Blood loss was monitored for 10 minutes via blood collected in pre-weighed gauze held adjacent to the injury, a 3x1.5 cm cut through the left lobe of the liver measured with a ruler prior to cutting. Gauze was changed every 10 seconds for 30 seconds, every 30 seconds until 3 minutes, and every minute until 10 minutes and weighed

immediately to quantify blood loss over time. Terminal cardiac puncture and organ/wound harvest was conducted. Platelet count, PPP isolation, and a fibrinogen ELISA was performed. MSB and IHC were performed on wound sections for fibrin (UC45) (GeneTex) and platelets (SJ19-09; Novus Biologicals). Confocal microscopy was utilized to examine fibrin clot structure of PPP and quantify fiber density from animals after injury as above.

DIC patient plasma clot structure

DIC patient plasma was obtained from Duke University Medical Center with IRB approval and informed consent from patients. Clots formed from three DIC patient's plasma were examined using confocal microscopy to visualize fibrin network properties and quantify fiber density and compare to normal human plasma clots. Clots from PPP were made with 1 U/mL thrombin and 0.05 mg/mL Alexa-Fluor 488 labeled fibrinogen, in HEPES buffer. FSNs, tPA-FSNs, or tPA-CS-IgGs (1mg/mL) were incorporated into DIC patient plasma clots prior to polymerization. Healthy adult human PPP used for controls was obtained from the New York blood center (New York, New York). Two duplicate clots were analyzed for each sample per condition, imaging and analyzing three images per duplicate.

Evaluation of clotting dynamics of DIC patient plasma in a microfluidic device under active coagulation

A custom-made Y-shaped microfluidic device was fabricated by soft lithography with channel cross-section of 500 x 234 μm. A stationary fibrin clot boundary was formed at the Y-junction with DIC patient plasma. Actively polymerizing flow solutions were flowed into the device for 20 minutes at wall shear rates of 10 s^{-1} containing corresponding DIC patient plasma. Images were taken over 20 minutes and clot boundary growth at the Y-junction was quantified.

Statistical analysis

Statistical analysis was performed in GraphPad Prism 8 (GraphPad, San Diego, CA, USA). Dextran release data was analyzed using multiple t-tests, two-tailed, correcting for multiple comparisons using the Holm-Sidak method with alpha=0.05. Other data sets were analyzed via a one-way analysis of variance (ANOVA) with a Tukey's post hoc test using a 95% confidence interval. Outlier tests were performed on all datasets prior to statistical analysis. All data is presented as average +/- standard deviation.

Data Sharing Statement: For original data, please contact aecarso2@ncsu.edu.

Results

Core-shell nanogels offer burst release profiles

Nanogels offer a tunable platform for drug delivery based on polymer network and crosslinking[33]. Poly(N-isopropylacrylamide), specifically, allows for complex architectures for customizable drug-delivery[38]. We have previously shown core-shell nanogel architectures with highly crosslinked cores facilitate partitioning of protein therapeutics into looser crosslinked shells for rapid release; we therefore utilized core-shell architecture here, comparing release dynamics to a single-layer nanogel[31]. Hydrodynamic core size and AFM diameter and height measurements increased from 170 +/- 17 nm, 166 +/- 16 nm, and 17 +/- 3 nm, respectively, to 287 +/- 67 nm, 263 +/- 28 nm, and 29 +/- 4 nm, upon shell addition. SEM images further validate shell addition (Figure 1). Hydrodynamic diameter and AFM diameter and height measurements for FSNs are similar to unconjugated counterparts, 239 +/- 55 nm, 254 +/- 61 nm and 25+/- 10 nm and for tPA-FSNs 225 +/- 53, 273 +/- 43, and 29 +/- 12 nm. Hydrodynamic diameter for CS-IgG particles shows similar size to fibrin-specific counterparts at 225 +/- 61 nm. FSNs display 67,200 +/- 3380 fibrin fragment E antibody molecules per particle. CS-IgG particles display 64,200 +/- 5580 sheep IgG isotype control molecules per particle.

To compare drug release, particle analysis verified single-layer 2% BIS crosslinked particles were similar in size to core-shell particles (268 +/- 34 nm). When loaded with 70kDa fluorescent dextran, mimicking tPA, releasate samples show core-shell particles offer a more burst release profile compared to single-layer nanogels such that a significantly larger percent of payload is delivered at early time points (Supplemental Figure 1). With applications for DIC where ischemic damage is a concern, burst release profiles are desired. Therefore, subsequent studies utilize core-shell particles. Once conjugated to a sheep antihuman fibrin fragment E antibody or a sheep IgG isotype control to make FSNs and CS-IgG particles respectively, tPA loading efficacy into the particles was determined to be 51 +/- 8.5 % and 46 +/- 7% for FSN and CS-IgG respectively (Figure 2A). Both FSN and CS-IgG particle types display burst release profiles over 44hrs (Figure 2B). Additionally, both FSNs and tPA-FSNs added to plasma, whole blood, and whole blood with 10% added complement serum did not show substantial particle aggregation (Supplemental Figure 2).

Fibrin-specific drug-loaded nanogels release functional tPA and lyse clots in vitro

Next, the functionality of fibrin-specific tPA-loaded particles was tested. Using an absorbance-based polymerization/degradation assay that was conducted under static conditions, tPA-FSNs exhibited a dual functionality in that they both promoted fibrin polymerization and degradation. TPA-FSN fluctuating absorbance values show fluctuating coagulations, indicating a modulation of polymerization and degradation not seen in controls. Importantly, the degradation characteristics observed through decreases in absorbance values, seen at 20 and 40 min, validate the release of functionally active tPA (Figure 2C).

We next investigated tPA-FSN's pro-coagulant and fibrinolytic action to pre-existing clots under conditions of flow that support fibrin polymerization to mimic DIC, particularly the pro-

thrombotic disease state where thrombin generation overpowers natural anti-coagulant/fibrinolytic pathways. Endpoint images and quantification of the stationary boundary clot growth show that under these dynamic conditions, in the controls, clot growth occurs at the boundary and minimal polymerization is observed in upstream channels (Figure 2D, E, Supplemental Figure 3). In the presence of unloaded FSNs, significant clot augmentation was observed. This was expected because unloaded FSNs target the clotting process by crosslinking fibrin fibers and assist in maturation of actively polymerizing clots[39]. Supplemental Figure 4 shows enhanced fiber density in the clot microstructure upon the addition of FSNs compared to control clot and clots with CS-IgG particles. C/S nanogels did not significantly alter clotting dynamics compared to controls and without active polymerization (+FSN and -Th), the effect FSNs have on clot augmentation is diminished. In the presence of tPA-FSNs, in actively polymerizing conditions, little upstream clotting and significantly less clot augmentation at the boundary is observed compared to controls as tPA-FSNs promote fibrinolytic action. This effect on clot lysis is more prominent than tPA alone or with non-targeted tPA-C/S particles and tPA-CS-IgG particles. Overall, these studies conducted under flow suggest tPA-FSNs can attenuate growing aberrant clot formations.

Microthrombi presentation is diminished and consumption of clotting factors is recovered in a rodent DIC model with tPA-FSN treatment

We next evaluated the ability of tPA-FSNs to modulate outcomes *in vivo* in a LPS-DIC model. DIC animals exhibited darkened organ color compared to control animals. MSB stained tissue sections also indicate microthrombi formations in DIC organs compared to controls, which is not as visible in tPA-FSN treated DIC animals. With the quantified fibrin IHC, significantly more microthrombi was seen in the heart, lung, liver, and kidney in DIC animals treated with saline or FSNs compared to controls (Figure 3A-E). However, significantly less microthrombi was seen

in the heart, lung, kidney, and liver in tPA-FSN treated animals, indicating fibrinolytic action from tPA-FSN treatment. Fewer microthrombi were also seen in tPA-CS-IgG treated DIC animals in the liver and lung. Organ weights are shown in Supplemental Figure 4 where heart, lung, and spleen had no differences. A significant kidney weight increase in DIC animals treated with saline, FSNs and tPA-FSNs was seen compared to controls. Also, a significant liver weight increase in DIC animals treated with saline, FSNs and tPA-FSNs was seen compared to DIC + tPA-CS-IgG particles.

When examining coagulation parameters, an increase in D-dimer in DIC animals compared to controls was observed (Figure 4E). No significant differences were seen in fibrinogen levels upon induction of DIC or following treatment with either saline, FSNs, or tPA-FSNs (Figure 4F). The elevated fibrin degradation product, and somewhat reduced fibrinogen levels, helps validate fibrin turnover and microthrombi formation in this model. Decreased platelet count is another hallmark of DIC, and upon LPS-induced DIC, animals treated with either saline, FSNs, or tPA-CS-IgGs showed significantly lower platelets counts compared to controls, indicating FSNs or tPA alone had little effect on circulating platelets. However, after treatment with tPA-FSNs, platelet count was recovered to control levels, indicating a recovery of the consumption of clotting factors known to occur in DIC (Figure 5G).

When evaluating the fibrin networks of clots formed from isolated plasma taken at the treatment endpoints, control animals formed robust clot networks with significantly higher fiber densities compared to DIC animals (Figure 4A, B), illustrating consumptive coagulopathy. FSN and tPA-CS-IgG treated DIC animals did not recover clotting structure. However, an increase in fiber density was observed with tPA-FSN treatment, suggesting recovery of clotting factor consumption in these DIC animals. A similar trend was seen analyzing *ex vivo* clots using

cryoSEM (Figure 4A, Supplemental Figure 5). Specifically, clots formed from plasma from DIC animals treated with saline, FSN and tPA-CS-IgG had a significantly higher percent porosity and lower intersection density compared to controls (Figure 4C-D), which was recovered in DIC animals treated with tPA-FSNs. Dot blots conducted with the plasma samples from control and DIC animals showed little presence of residual particles (Supplemental Figure 6). Additionally, exogenous addition of FSNs or tPA-FSNs to PPP from DIC + Saline PPP showed no improvement of clot structure, suggesting improvements in the clot structure observed are due to the particles influence on consumptive coagulopathy while in circulation, and not due to residual particles in the plasma. Clotting characteristics of plasma samples from control and DIC animals shows the consumption of clotting factors in DIC was apparent in this model, as DIC animals formed very poor clots *ex vivo*. However, clot structure was restored in animals receiving tPA-FSNs, demonstrating the therapeutic efficacy of tPA-FSNs in this model. The biodistribution of these particles (Supplemental Figure 7) observed after 30 minutes, shows a substantial presence of tPA-FSNs and FSNs in the kidney. Additionally, tPA-FSNs and FSNs particles were detected in the lung. To some extent, FSNs were detected in the heart and liver, and tPA-FSNs were detected in the spleen. Dot blot analysis shows significantly higher tPA-FSNs in whole blood samples compared to FSNs, and presence of tPA-FSNs in the urine.

tPA-FSN treatment improved bleeding outcomes in DIC rodent model

To directly evaluate tPA-FSN's influence on bleeding risks associated with DIC, the LPS-DIC model was used in conjunction with a well-established liver injury bleeding model. Compared to control and vehicle groups, DIC induced animals treated with saline, FSNs, or tPA-CS-IgGs bled more over time and had significantly higher total blood loss (Figure 5A,B). tPA-FSN treatment significantly decreased bleeding compared to tPA-CS-IgG and there was no longer a

significantly higher blood loss compared to control or vehicle groups (Figure 5A, B). MSB staining at the wound shows robust collagen and fibrin incorporation in tPA-FSN treatment groups (Figure 5C). IHC fibrin quantification shows significantly higher fibrin incorporation at the wound in DIC animals treated with tPA-FSNs compared to other DIC animals (Figure 5D). CD61 quantification shows that DIC animals treated with saline, FSNs, or tPA-CS-IgGs had significantly less platelets at the wound site compared to control, vehicle, or tPA-FSN treated DIC animals (Figure 5E). When coupled with this injury model, fibrinogen levels for saline, tPA-FSN, and tPA-CS-IgG treated DIC animals were significantly lower than vehicle controls (Figure 5F), suggesting ongoing DIC or fibrinogen consumption at the wound sites. No significant differences were observed in platelet counts (Figure 5G). Additionally, clotting capability from plasma samples post-injury was significantly reduced in the DIC animals treated with saline, FSNs, tPA-CS-IgGs, or vehicle controls, compared to control animals. However, tPA-FSN treated DIC animals had robust clotting capabilities post-injury with significantly higher fiber density compared to other DIC animals (Figure 5H,I). Taken together, these data further demonstrate the ability of tPA-FSNs to improve bleeding outcomes in a DIC model potentially due to ameliorating consumptive coagulopathy.

DIC patient plasma clot structure

To translate these therapeutic effects to human patients, nanogels were added to three DIC patient's plasma samples *ex vivo* to evaluate clot structure. The average fibrinogen level in these DIC patients was 335 +/- 256 mg/dL, D-dimer levels 79,036 +/- 29,648 ng/mL, prothrombin time 23.7 +/- 3.2 sec, prothrombin INR 2.0 +/- 0.3, activated partial thromboplastin time 48.0 +/- 23.3 sec, and platelet count 53,500 +/- 9,192 platelets/μL. Individual values are shown in Supplemental Table 1. Fibrin network properties of DIC patient plasma samples show heterogenous clot structure with significantly higher fiber densities when compared to controls (Figure 6A, B). Unloaded

FSNs did not alter clot structure or fiber density, however, the addition of tPA-FSNs resulted in more homogenous clot structures with reduced fiber density and more closely resembled control clots. Whereas the addition of tPA-CS-IgG particles showed areas of clot lysis mixed with highly heterogenous areas of dense clot formation resulting in highly variable fiber density measurements. Therefore, in this DIC patient population, tPA-FSN treatment could potentially be used to recover clotting capabilities similar to healthy human plasma.

Evaluation of clotting dynamics of DIC patient plasma in microdevice under active coagulation

After examining static conditions, DIC patient plasma was then incorporated into a microfluidic device to see tPA-FSN efficacy under dynamic conditions. Under flow, baseline DIC patient plasma samples showed significantly higher clot growth at the stationary clot boundary site compared to controls, which was significantly decreased upon the addition of tPA-FSNs (Figure 6E). During coagulation under flow, DIC patient plasma also exhibited thrombosis in upstream channels (Figure 6D), in some instances *in situ* thrombus formation blocked flow. This was not observed in control human plasma samples or in DIC samples with tPA-FSNs. Overall, these fluidic conditions with patient plasma confirms the extensive disease state of DIC, where thrombosis is a critical concern. tPA-FSN incorporation in these studies indicates a potential therapeutic to mitigate thrombosis risks in this patient population.

Discussion

Through these studies, fibrin-targeting nanogels have been utilized to release tPA as a therapeutic strategy to treat widespread clotting and fibrin deposition in circumstances of DIC. The fibrin-targeting potential of FSNs has been shown to augment clotting dynamics in conditions of active polymerization, which itself can aid in fibrin polymerization in circumstances of bleeding

risks. With tPA-FSNs, fibrin-directed fibrinolysis was shown to more effectively lyse clots compared to undirected fibrinolytic action *in vitro*. *In vivo*, tPA-FSNs reduced microthrombi presentation, improved clot structure, and improved bleeding outcomes in LPS-induced DIC to a higher degree than their untargeted counterpart. tPA treatment in untargeted particles, while effective at reducing microthrombi presentation in some organs, did not improve bleeding outcomes. While a number of sepsis-induced DIC models could be considered, to varying levels of physiological relevance, the LPS-induced model replicated the thrombotic and consumptive coagulopathy of DIC in rodents to which tPA-FSNs were designed to target[36,40–42]. LPS-induced models display suppressed fibrinolytic-type DIC, similar to DIC types seen in sepsis[36]. However, LPS-induced DIC models do not mimic all of the complex physiological responses to sepsis in human patients. For example, the rapid transient increase in cytokines displayed in the LPS-induced DIC model differ from human sepsis[40–42]. In future studies, a cecal ligation and puncture (CLP) model could be included to further support tPA-FSN efficacy in sepsis-induced thrombosis. Along with the alternative animal model consideration for future studies, blinded observations and randomized treatment allocation will be necessary to confirm therapeutic efficacy. Limitations in the presented study include unconscious bias due to unblinded observations.

The data presented in this study support the premise that tPA-FSNs can inhibit both microthrombi formation in organs and bleeding risks associated with DIC. In circumstances of consumptive coagulopathy, with reduced platelets and clotting factors, tPA-FSNs may hone to aberrant microthrombi formations, lysing the clot to restore clotting factors such as platelets and restore consumptive coagulopathy, seen in Figure 4A-D and 4G. Additionally, tPA-FSNs may bind to and prevent the growth of actively forming thrombi, seen *in vitro* in Figure 2D-E and 6D-E, deterring further consumption of clotting factors. Indeed, when presented with an injury, DIC

animals treated with tPA-FSNs exhibited blood loss comparable to controls. The decrease in bleeding compared to other DIC animals treated with saline, unloaded FSNs, or untargeted tPA delivery, can be attributed to the action of the tPA-FSNs prior to injury and their ability to recover consumptive coagulopathy. Systemic spillover of tPA is possible, however, with a nanogel delivery approach potential spillover is limited to sub-therapeutic doses where increased bleeding was not observed. In human DIC patient samples, heterogenous clot networks with areas of extremely high fiber densities demonstrate a prothrombotic disease state, perhaps prior to any consumption of clotting factors that can lead to bleeding complications. Under such circumstances, circulating tPA-FSNs can work to target fibrinolytic action in areas where high fiber density, or high fibrin content, can cause disruptive microthrombi formation when *in vivo*. By mitigating these risks of aberrant clot formation with targeted fibrinolytic action, tPA-FSNs, can potentially reduce thrombosis risks in this patient population. The timing of this therapeutic during progression of DIC should be thoughtfully considered and may not be appropriate in cases of active bleeding.

Anticoagulant therapies specifically have been studied to treat DIC. For example, antithrombin III (ATIII), when used without concomitant heparin, showed reduced mortality rates at 90 days, although with concomitant heparin, mortality did not differ between ATIII and placebo treatment[30]. Also, bleeding incidences did increase with ATIII treatment, which is a crucial concern for DIC[30]. Reducing dosage of ATIII showed some promising results in improved 28 day mortality[43]. By administering a more targeted fibrinolytic therapeutic, such as the tPA-FSNs examined in this study, bleeding risks would be attenuated since fibrinolytic action is localized to areas of fibrin accumulation and not off-target sites, and thus lower doses would inherently be required compared to systemic therapies. Additionally, compared to ATIII therapies, tPA-FSNs would have the ability to eliminate pre-existing aberrant microthrombi and not just new

coagulation activity. Compared to heparin treatment, which in itself may only be suitable in certain condition of DIC, tPA-FSNs may offer reduced risks of off-target bleeding as well[14,44]. Experimental treatments involving the thrombomodulin and protein C system, another strategy geared towards replenishing native coagulation inhibitory mechanism in the coagulation pathway, have shown mixed results, with some studies reporting increased incidence of hemorrhage-related events, which again can be mitigated with a fibrin-targeted approach of tPA-FSNs[26,45–47]. Important considerations for drug-delivery systems used to treat thrombotic complications by delivering antithrombotic agents have been reviewed[48], and studied for applications of thromboprophylaxis as well[49–52], which show promise preventing thrombosis and providing protection against endotoxemia. TPA-FSNs may act additionally to direct therapeutic treatment, lysing existing aberrant thrombi and preventing further exacerbation of coagulation factors, following initial onset of systemic coagulopathy.

This work has the potential to significantly improve treatment options for DIC patients. Although the coagulopathies associated with COVID-19 display distinct features compared to DIC, critically ill patients can progress to DIC due to additional secondary infections, and that are associated with higher mortality rates[53–55]**.** Early work on administering anticoagulant treatment (e.g. heparin) in COVID-19 patients with coagulopathy shows promise in reducing mortality, and these effects seem to be positively correlated with D-dimer levels[55]. Also, a case series of tPA treatment for COVID-19 patients with acute respiratory distress syndrome showed initial improvements in lung function, although not sustained after tPA treatment[56]. Since microcirculatory clot formation seems to be a prominent cause of acute lung injury and mortality in COVID-19 patients[57], tPA-FSNs may offer a novel therapeutic approach in this patient population, that could offer targeted delivery of fibrinolytic agents to lyse aberrant clots in the

microcirculation to mitigate organ damage, and potentially improve coagulopathy in this patient population.

These findings provide increased evidence for the need to develop targeted fibrinolytic strategies to treat thrombotic complications, including DIC, especially by targeting to pre-existing fibrin. Next steps in this therapy should involve thorough safety analyses, including dosing studies. With a tunable nanogel platform that allows for multidrug encapsulation, dual-loaded studies with multiple therapeutics could be examined for enhanced therapeutic efficacy, especially directly related to mitigating the excessive thrombin generation causing DIC. In conclusion, this study has shown that fibrin-targeting nanogels delivering tPA can help dissolve aberrant fibrin deposition to restore coagulation potential and thus mitigate thrombosis and bleeding complications of DIC to potentially improve outcomes.

Acknowledgements

Funding for this project was provided by National Science Foundation CAREER DMR (1847488), the National Institute of Health NHLBI (R01HL146701), the North Carolina Biotechnology Center Flash grant and an American Heart Association Predoctoral Fellowship (18PRE33990338) to EM. We would also like to acknowledge E. Johannes and the Cellular and Molecular Imaging Facility for assistance with confocal microscopy and C. Zhou and the Analytical Instrumentation Facility (AIF) at North Carolina State University.

Author Contributions and Conflict of Interest Disclosures

E.M. conducted particle synthesis and characterization, *in vitro* stationary and fluidic clotting dynamics experimentation, *in vivo* studies with and without injury and subsequent analysis in these

animal models, DIC patient sample microscopy and fluidic device experimentation, and paper writing. M.S. performed release studies comparing core-shell and single-layer particles, aided in particle synthesis and paper writing and *in vivo* studies with the injury model. N.M. conducted T-junction PDMS device fabrication and aided in T-junction device experimentation and paper writing. K.N. aided in *in vivo* studies and conducted confocal microscopy in the DIC model without injury. G.K. and J.L. acquired DIC patient plasma. M.D. and H.D. supervised and fabricated microfluidic devices. ACB designed and supervised the study, data analysis, and paper writing. The authors declare no competing financial interests.

References

1. Sivula M, Tallgren M, Pettilä V. Modified score for disseminated intravascular coagulation in the critically ill. *Intensive Care Med.* 2005;31(9):1209–1214.
2. Bakhtiari K, Meijers J, Jonge E de, Levi M. Prospective validation of the International Society of Thrombosis and Haemostasis scoring system for disseminated intravascular coagulation*. *Crit. Care Med.* 2004;32(12):2416–2421.
3. Cartin-Ceba R, Kojicic M, Li G, et al. Epidemiology of Critical Care Syndromes, Organ Failures, and Life-Support Interventions in a Suburban US Community. *Chest*. 2011;140(6):1447–1455.
4. Toh C, Downey C. Performance and prognostic importance of a new clinical and laboratory scoring system for identifying non-overt disseminated intravascular coagulation. *Blood Coagul. Fibrinolysis*. 2005;16(1):69–74.
5. Levi M, ten Cate H. Disseminated Intravascular Coagulation. *N. Engl. J. Med.* 1999;341(8):586–592.
6. Bick RL. Disseminated intravascular coagulation: a review of etiology, pathophysiology, diagnosis, and management: guidelines for care. *Clin. Appl. Thromb. Off. J. Int. Acad. Clin. Appl. Thromb.* 2002;8(1):1–31.
7. Iba T, Levy JH, Raj A, Warkentin TE. Advance in the Management of Sepsis-Induced Coagulopathy and Disseminated Intravascular Coagulation. *J. Clin. Med.* 2019;8(5):728.
8. Connors JM, Levy JH. Thromboinflammation and the hypercoagulability of COVID-19. *J. Thromb. Haemost.* 2020;jth.14849.
9. Connors JM, Levy JH. COVID-19 and its implications for thrombosis and anticoagulation. *Blood*. 2020;135(23):2033–2040.
10. Levi M, Thachil J, Iba T, Levy JH. Coagulation abnormalities and thrombosis in patients with COVID-19. *Lancet Haematol.* 2020;7(6):e438–e440.
11. Iba T, Levy JH, Levi M, Connors JM, Thachil J. Coagulopathy of Coronavirus Disease 2019. *Crit. Care Med.* 2020;48(9):1358–1364.

12. Hayakawa M, Saito S, Uchino S, et al. Characteristics, treatments, and outcomes of severe sepsis of 3195 ICU-treated adult patients throughout Japan during 2011–2013. *J. Intensive Care*. 2016;4(1):44.
13. Iba T, Umemura Y, Watanabe E, et al. Diagnosis of sepsis-induced disseminated intravascular coagulation and coagulopathy. *Acute Med. Surg.* 2019;6(3):223–232.
14. Levi M, Scully M. How I treat disseminated intravascular coagulation. *Blood*. 2018;131(8):845–854.
15. Boral BM, Williams DJ, Boral LI. Disseminated Intravascular Coagulation. *Am. J. Clin. Pathol.* 2016;146(6):670–680.
16. Gando S, Levi M, Toh C-H. Disseminated intravascular coagulation. *Nat. Rev. Dis. Primer*. 2016;2:16037.
17. Varga Z, Flammer AJ, Steiger P, et al. Endothelial cell infection and endotheliitis in COVID-19. *Lancet Lond. Engl.* 2020;395(10234):1417–1418.
18. Iba T, Levy JH, Warkentin TE, et al. Diagnosis and management of sepsis-induced coagulopathy and disseminated intravascular coagulation. *J. Thromb. Haemost.* 2019;17(11):1989–1994.
19. Matsuda T. Clinical aspects of DIC--disseminated intravascular coagulation. *Pol. J. Pharmacol.* 1996;48(1):73–75.
20. Weisel JW, Litvinov RI. Mechanisms of fibrin polymerization and clinical implications. *Blood*. 2013;121(10):1712–1719.
21. Kattula S, Byrnes JR, Wolberg AS. Fibrinogen and fibrin in hemostasis and thrombosis. *Arterioscler. Thromb. Vasc. Biol.* 2017;37(3):e13–e21.
22. Falati S, Gross P, Merrill-Skoloff G, Furie BC, Furie B. Real-time in vivo imaging of platelets, tissue factor and fibrin during arterial thrombus formation in the mouse. *Nat. Med.* 2002;8(10):1175–1180.
23. La Corte ALC, Philippou H, Ariëns RAS. Chapter 3 - Role of Fibrin Structure in Thrombosis and Vascular Disease. *Adv. Protein Chem. Struct. Biol.* 2011;83:75–127.
24. Gallino A, Haeberli A, Baur H R, Straub P W. Fibrin formation and platelet aggregation in patients with severe coronary artery disease: relationship with the degree of myocardial ischemia. *Circulation*. 1985;72(1):27–30.
25. Undas Anetta, Podolec Piotr, Zawilska Krystyna, et al. Altered Fibrin Clot Structure/Function in Patients With Cryptogenic Ischemic Stroke. *Stroke*. 2009;40(4):1499–1501.
26. Levi M, de Jonge E, van der Poll T. New treatment strategies for disseminated intravascular coagulation based on current understanding of the pathophysiology. *Ann. Med.* 2004;36(1):41–49.
27. Jackson SP, Darbousset R, Schoenwaelder SM. Thromboinflammation: challenges of therapeutically targeting coagulation and other host defense mechanisms. *Blood*. 2019;133(9):906–918.
28. Anglés-Cano E. Overview on fibrinolysis: Plasminogen activation pathways on fibrin and cell surfaces. *Chem. Phys. Lipids*. 1994;67–68:353–362.
29. Hoylaerts M, Rijken DC, Lijnen HR, Collen D. Kinetics of the activation of plasminogen by human tissue plasminogen activator. Role of fibrin. *J. Biol. Chem.* 1982;257(6):2912–2919.
30. Warren BL, Eid A, Singer P, et al. High-Dose Antithrombin III in Severe Sepsis: A Randomized Controlled Trial. *JAMA*. 2001;286(15):1869–1878.

31. Mihalko E, Huang K, Sproul E, Cheng K, Brown AC. Targeted Treatment of Ischemic and Fibrotic Complications of Myocardial Infarction Using a Dual-Delivery Microgel Therapeutic. *ACS Nano*. 2018;12(8):7826–7837.
32. Blackburn WH, Dickerson EB, Smith MH, McDonald JF, Lyon LA. Peptide-Functionalized Nanogels for Targeted siRNA Delivery. *Bioconjug. Chem.* 2009;20(5):960–968.
33. Oh JK, Drumright R, Siegwart DJ, Matyjaszewski K. The development of microgels/nanogels for drug delivery applications. *Prog. Polym. Sci.* 2008;33(4):448–477.
34. Sproul EP, Hannan RT, Brown AC. Controlling Fibrin Network Morphology, Polymerization, and Degradation Dynamics in Fibrin Gels for Promoting Tissue Repair. *Biomater. Tissue Eng. Methods Protoc.* 2018;85–99.
35. Asakura H, Suga Y, Yoshida T, et al. Pathophysiology of disseminated intravascular coagulation (DIC) progresses at a different rate in tissue factor-induced and lipopolysaccharide-induced DIC models in rats. *Blood Coagul. Fibrinolysis*. 2003;14(3):221.
36. Asakura H. Classifying types of disseminated intravascular coagulation: clinical and animal models. *J. Intensive Care*. 2014;2(1):20.
37. Morgan CE, Prakash VS, Vercammen JM, Pritts T, Kibbe MR. Development and validation of 4 different rat models of uncontrolled hemorrhage. *JAMA Surg.* 2015;150(4):316–324.
38. Smith MH, Lyon LA. Multifunctional Nanogels for siRNA Delivery. *Acc. Chem. Res.* 2012;45(7):985–993.
39. Brown AC, Stabenfeldt SE, Ahn B, et al. Ultrasoft microgels displaying emergent, platelet-like, behaviors. *Nat. Mater.* 2014;13(12):1108–1114.
40. Mai S, Khan M, Liaw P, Fox-Robichaud A. Experimental Sepsis Models. *Sepsis - Ongoing Signif. Chall.* 2012;
41. Beristain-Covarrubias N, Perez-Toledo M, Thomas MR, et al. Understanding Infection-Induced Thrombosis: Lessons Learned From Animal Models. *Front. Immunol.* 2019;10:.
42. Dejager L, Pinheiro I, Dejonckheere E, Libert C. Cecal ligation and puncture: the gold standard model for polymicrobial sepsis? *Trends Microbiol.* 2011;19(4):198–208.
43. Iba T, Saitoh D, Wada H, Asakura H. Efficacy and bleeding risk of antithrombin supplementation in septic disseminated intravascular coagulation: a secondary survey. *Crit. Care*. 2014;18(5):497.
44. Zarychanski R, Abou-Setta A, Kanji S, et al. Efficacy and safety of heparin in patients with sepsis: a systematic review and meta-analysis. *Crit. Care*. 2015;19(1):P123.
45. Ikezoe T. Thrombomodulin/activated protein C system in septic disseminated intravascular coagulation. *J. Intensive Care*. 2015;3(1):.
46. Opal SM, LaRosa SP. Recombinant Human Activated Protein C as a Therapy for Severe Sepsis: Lessons Learned? *Am. J. Respir. Crit. Care Med.* 2013;187(10):1041–1043.
47. Bernard GR, Vincent JL, Laterre PF, et al. Efficacy and safety of recombinant human activated protein C for severe sepsis. *N. Engl. J. Med.* 2001;344(10):699–709.
48. Greineder CF, Howard MD, Carnemolla R, Cines DB, Muzykantov VR. Advanced drug delivery systems for antithrombotic agents. *Blood*. 2013;122(9):1565–1575.
49. Villa CH, Pan DC, Johnston IH, et al. Biocompatible coupling of therapeutic fusion proteins to human erythrocytes. *Blood Adv.* 2018;2(3):165–176.
50. Carnemolla R, Villa CH, Greineder CF, et al. Targeting thrombomodulin to circulating red blood cells augments its protective effects in models of endotoxemia and ischemia-reperfusion injury. *FASEB J. Off. Publ. Fed. Am. Soc. Exp. Biol.* 2017;31(2):761–770.

51. Zaitsev S, Kowalska MA, Neyman M, et al. Targeting recombinant thrombomodulin fusion protein to red blood cells provides multifaceted thromboprophylaxis. *Blood*. 2012;119(20):4779–4785.
52. Zaitsev S, Spitzer D, Murciano J-C, et al. Sustained thromboprophylaxis mediated by an RBC-targeted pro-urokinase zymogen activated at the site of clot formation. *Blood*. 2010;115(25):5241–5248.
53. Tang N, Li D, Wang X, Sun Z. Abnormal coagulation parameters are associated with poor prognosis in patients with novel coronavirus pneumonia. *J. Thromb. Haemost.* 2020;18(4):844–847.
54. Han H, Yang L, Liu R, et al. Prominent changes in blood coagulation of patients with SARS-CoV-2 infection. *Clin. Chem. Lab. Med.* 2020;58(7):1116–1120.
55. Tang N, Bai H, Chen X, et al. Anticoagulant treatment is associated with decreased mortality in severe coronavirus disease 2019 patients with coagulopathy. *J. Thromb. Haemost.* 2020;18(5):1094–1099.
56. Wang J, Hajizadeh N, Moore EE, et al. Tissue plasminogen activator (tPA) treatment for COVID-19 associated acute respiratory distress syndrome (ARDS): A case series. *J. Thromb. Haemost. JTH*. 2020;
57. Fox SE, Akmatbekov A, Harbert JL, et al. Pulmonary and Cardiac Pathology in Covid-19: The First Autopsy Series from New Orleans. *medRxiv*. 2020;2020.04.06.20050575.

Figures

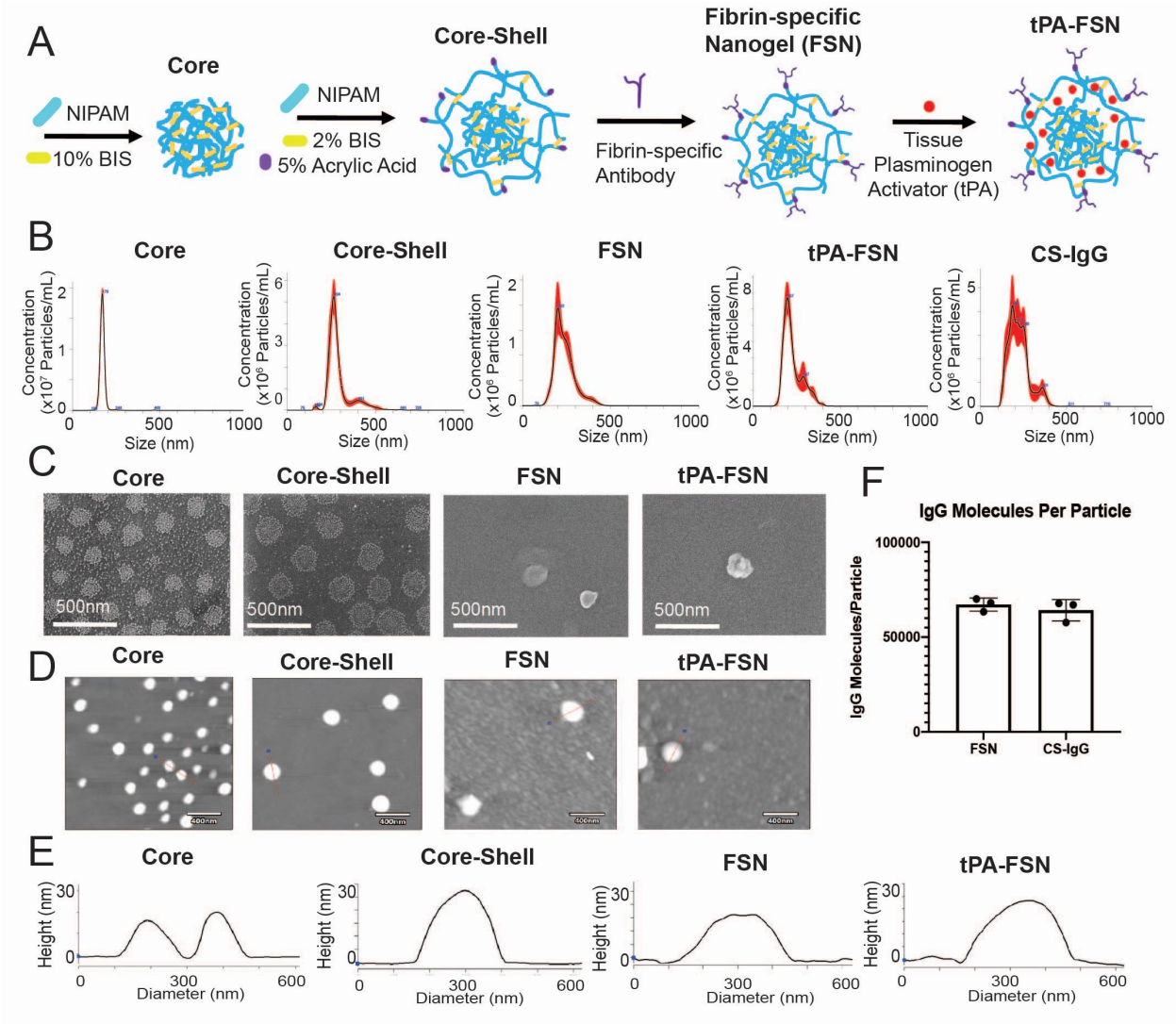

Figure 1: **Nanogel synthesis schematic and characterization.** Schematic of core-shell particle synthesis and FSN fabrication followed by subsequent tPA loading through a rehydration technique (**A**). Core, core-shell, FSN, tPA-FSN, and tPA-CS-IgG size characterization hydrodynamic measurements (n=10^8 particles) (**B**). Scanning electron microscopy (JEOL JSM-7600F) images are shown at 80,000x magnification to validate core-shell architecture and FSN and tPA-FSN structure (**C**). atomic force microcopy (AFM; Asylum Research MFP-3D) dry images (n=30 particles) with representative images shown (**D**) and height traces (n=30 particles;

representative images shown) (**E**). Quantification of antibody molecules per particle for FSN and CS-IgG particles (**F**).

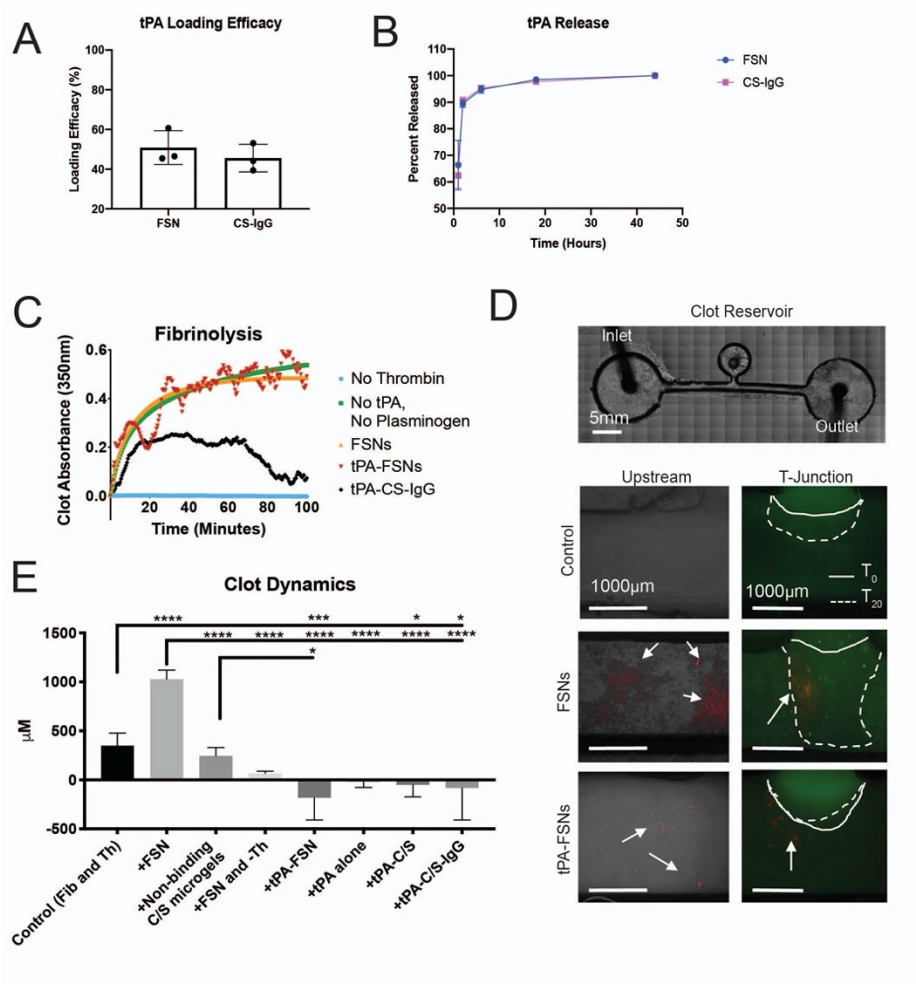

Figure 2: *In vitro* evaluation of drug release characteristics and clotting under static and dynamic conditions. tPA loading and release studies comparing core-shell FSN and CS-IgG particles (**A**) (n=3). Absorbance-based polymerization-degradation (**B**) with tPA loaded into core-shell FSN particles (n=3). *In vitro* clotting under dynamic conditions in a fluidic device (**C**) contained a stationary fibrin clot located in the clot reservoir and flow solutions with fibrinogen and thrombin (control) (n=7), fibrinogen and thrombin with unloaded FSNs (n=4), fibrinogen and thrombin with non-binding core-shell nanogels (n=3), fibrinogen with unloaded FSNs without

thrombin and thus no active coagulation (n=3), fibrinogen and thrombin with tPA-FSNs (n=4), fibrinogen and thrombin with tPA alone (n=3), and fibrinogen and thrombin with tPA loaded into non-binding core-shell nanogels (n=3) and tPA-CS-IgG (n=3). Alexa-Fluor 488 labeled fibrinogen was used in all fibrinogen solutions and the stationary clot. All nanogels used are fluorescently labeled (rhodamine B) and arrows point to present nanogels in fluidic device above. Images were taken on an EVOS FL Auto Imaging System at 4x magnification and remaining conditions are shown in Fig. S1. Solid line represents initial clot boundary and the dotted line represents the clot boundary after 20 minutes of flow at a wall shear rate of 1 s^{-1}, which was used to quantify clot growth (**D**). Quantification was conducted on ImageJ software. Data is presented as average +/- standard deviation. Clot dynamics were analyzed via a one-way analysis of variance (ANOVA) with a Tukey's post hoc test using a 95% confidence interval. *$p<0.05$, **$p<0.01$, ****$p<0.0001$.

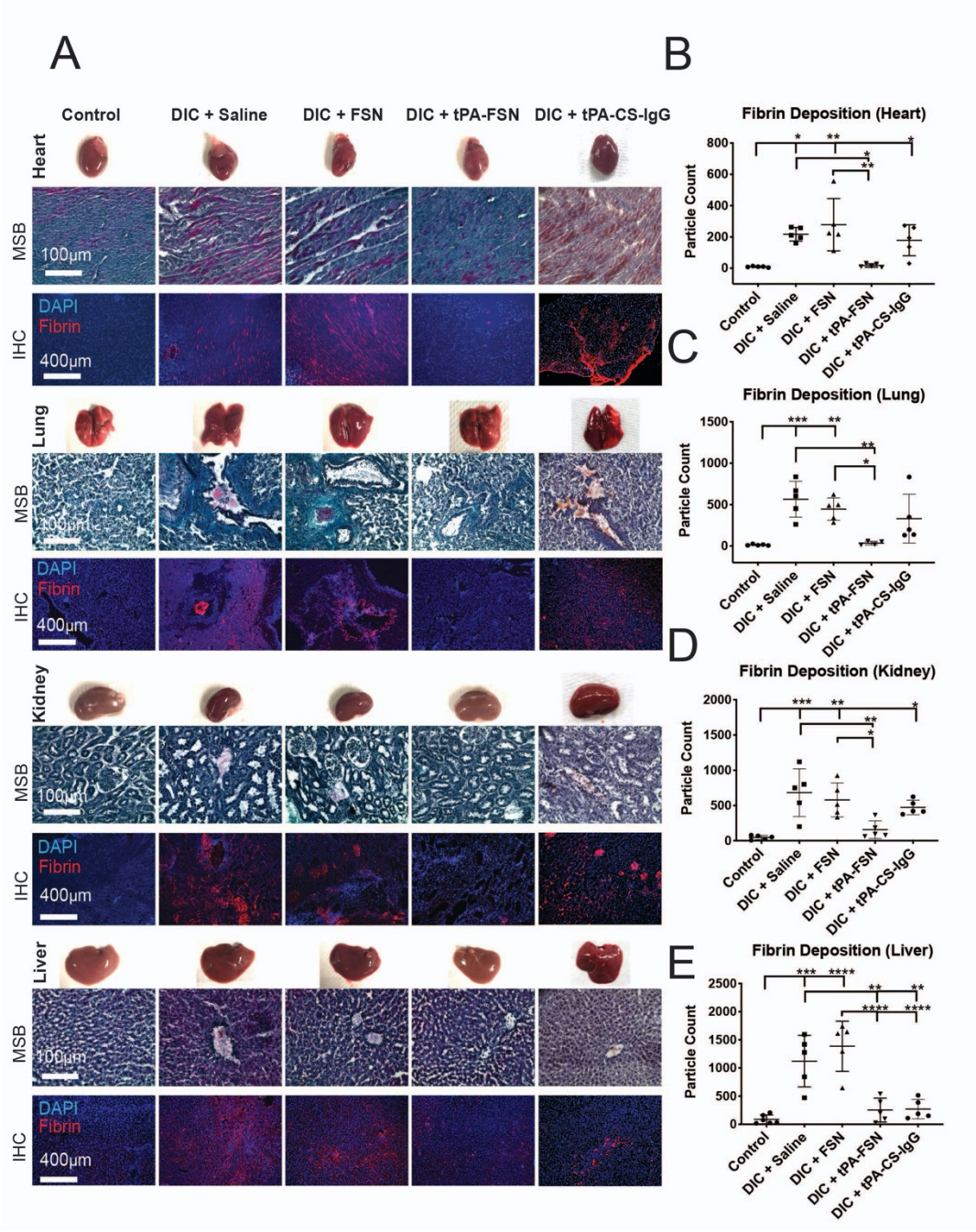

Figure 3: *In vivo* microthrombi examination in a DIC rodent model. LPS induced DIC rodent model harvested organs including heart, lung, kidney, and liver with corresponding whole organ pictures, MSB stained tissue sections, and immunohistochemistry for fibrin deposition in tissue sections are shown (**A**). DIC animals were treated with saline (n=5), unloaded FSNs (n=5), tPA-FSNs (n=5) and tPA-CS-IgG (n=5) are compared to controls (n=6). Images were taken on an

EVOS FL Auto Imaging System at 10x magnification. Corresponding quantification, conducted with ImageJ particle analysis software, for immunohistochemistry of fibrin deposition in the heart (**B**), lung (**C**), kidney (**D**), and liver (**E**) tissue sections was averaged for three images per organ tissue section for each animal (n=6 for control liver, n=4 for DIC + tPA-FSN lung, 5 for all other groups). Data is presented as average +/- standard deviation. Data sets were analyzed via a one-way analysis of variance (ANOVA) with a Tukey's post hoc test using a 95% confidence interval. *p<0.05, **p<0.01, ***p<0.001, ****p<0.0001.

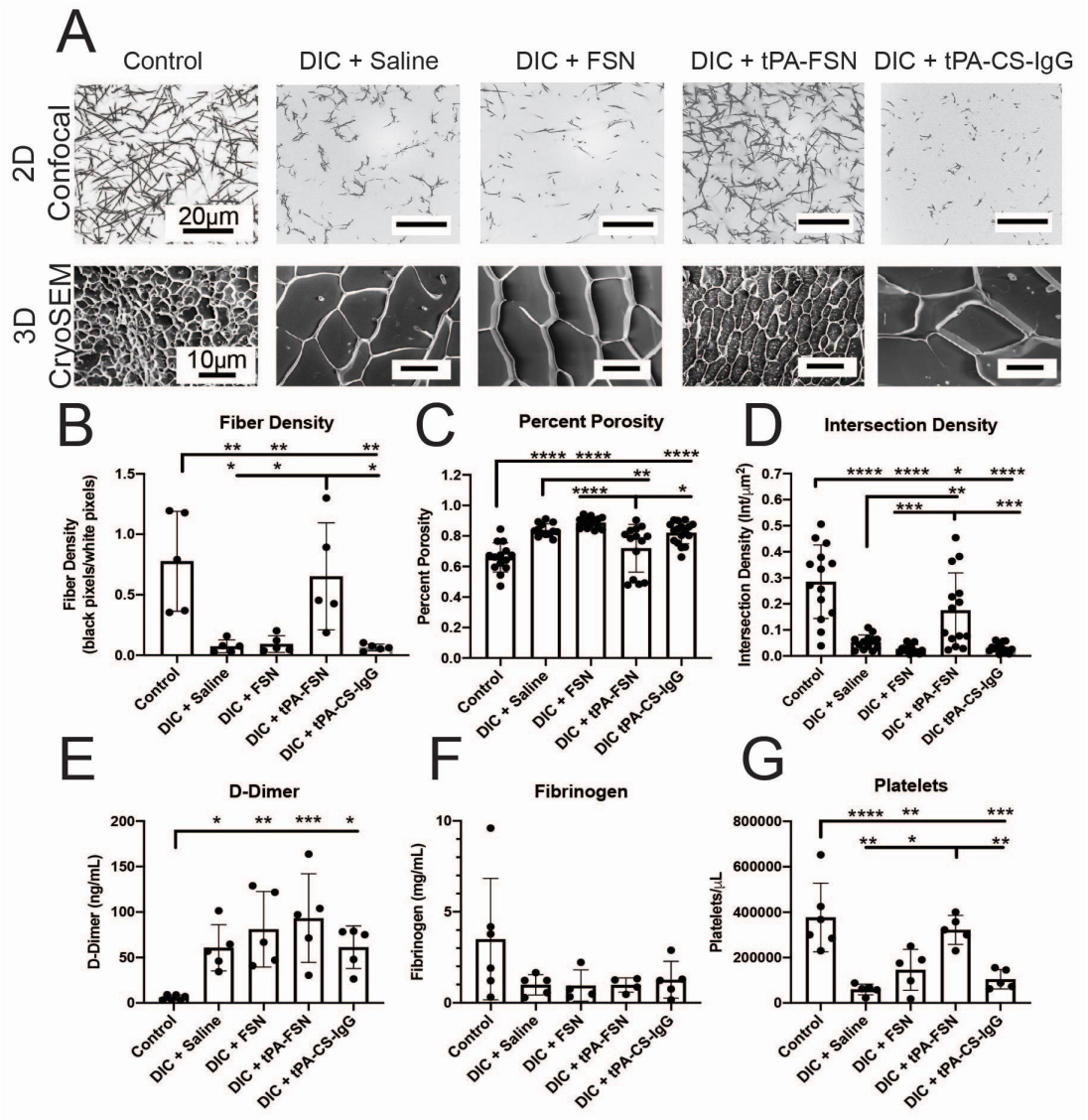

Figure 4: Examination of clotting characteristics and coagulation parameters from a DIC rodent model. Clot formation from control and DIC animals treated with saline, FSNs, tPA-FSNs, or tPA-CS-IgG particles through confocal microscopy (top) and cryoSEM (bottom) (**A**). A Zeiss Laser Scanning Microscope (LSM 710, Zeiss Inc., White Plains, NY, USA) was used for confocal images. 1.89 μm z-stack images were taken with objective C-Apochromat 63x 1.2W. Images were analyzed using ImageJ to make 8-bit 3D projections of z-stack images. Fiber density was quantified by determining the ratio of black (fiber) over white (background) pixels in each binary image. (average of three images per animal) (n=5 for all groups). Clot structure via cryoSEM was conducted using a JEOL 7600F cryogenic SEM (cryoSEM) with a Gatan Alto Cryo-transfer system. All images were taken at 2500x magnification. Quantification was conducted using DiameterJ plugin on ImageJ software. Corresponding quantification is shown for fiber density from confocal microscopy (**B**), and percent porosity (**C**) and intersection density (**D**) quantification from cryoSEM images (2 or 3 images per animal, n=6 control animals, 5 animals for all DIC groups). D-dimer (**E**) and fibrinogen (**F**) quantification from plasma samples taken from control (n=6) and DIC animals (n=4 for DIC + FSN and DIC + tPA-FSN groups fibrinogen levels, n=5 for all other groups). Platelet count from control and DIC animals (n=6 for control, n=5 for all other groups) (**G**). All data is presented as average +/- standard deviation. Data sets were analyzed via a one-way analysis of variance (ANOVA) with a Tukey's post hoc test using a 95% confidence interval. *$p<0.05$, **$p<0.01$, ***$p<0.001$, ****$p<0.0001$.

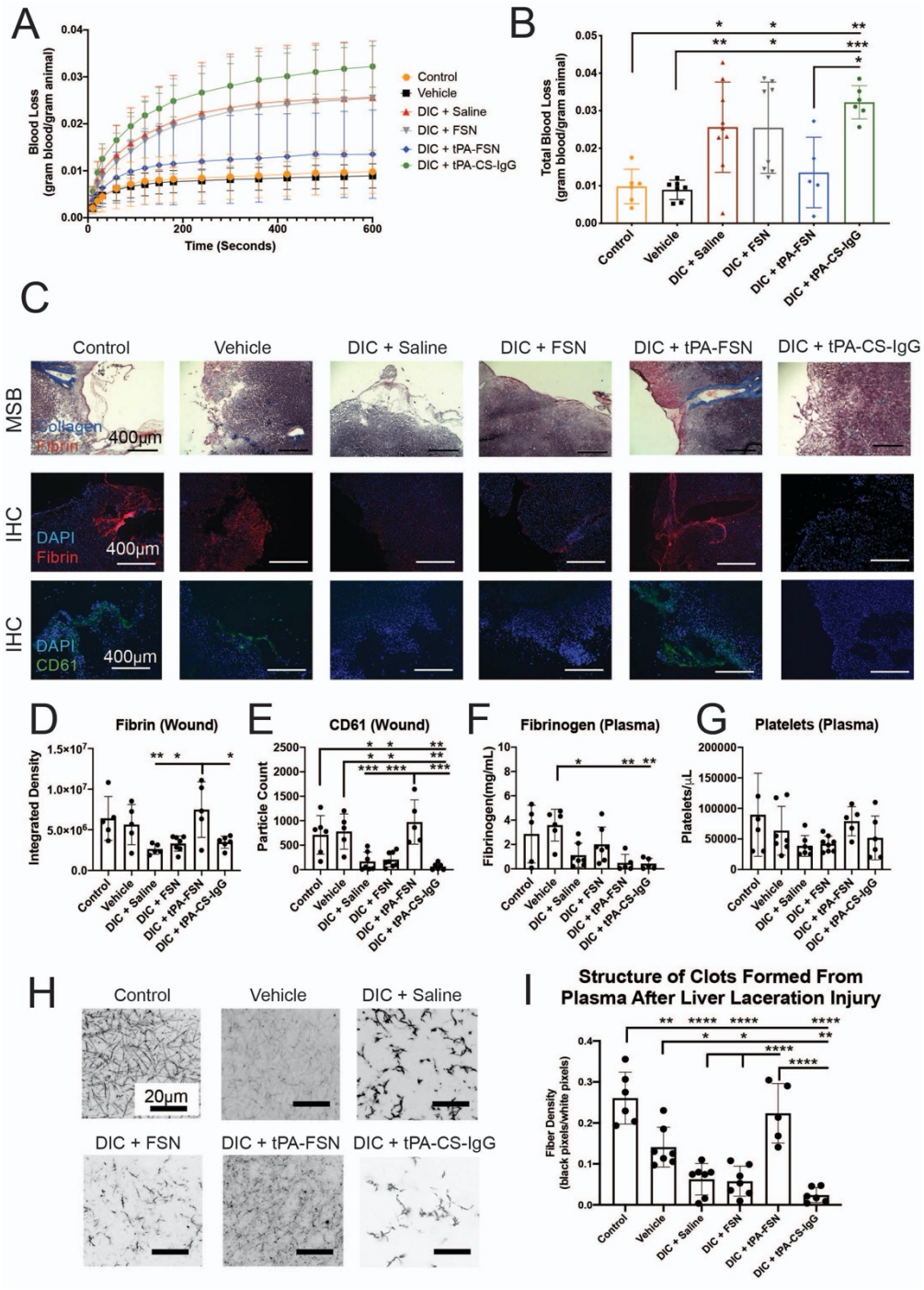

Figure 5: Evaluation of bleeding in a DIC rodent model with tPA-FSN treatment. Blood loss over time (**A**) and total blood loss (**B**) from control (n=6), vehicle (n=7), and DIC animals treated with either saline (n=9), FSNs (n=8), tPA-FSNs (n=5), or tPA-CS-IgG (n=6) from a liver laceration injury. Representative histology images from wound tissue sections from each treatment

group including MSB stained wound sections, immunohistochemistry for fibrin at the wound site, and immunohistochemistry for CD61 at the wound site (**C**). Images were taken on an EVOS FL Auto Imaging System at 10x magnification. Corresponding quantification was conducted with ImageJ particle analysis software. Fibrin IHC quantification (control (n=5), vehicle (n=5), DIC + saline (n=5), DIC + FSN (n=7), DIC + tPA-FSN (n=5), DIC + tPA-CS-IgG (n=6)) (**D**) and platelet (CD61) IHC quantification (control (n=6), vehicle (n=5), DIC + saline (n=7), DIC + FSN (n=8), DIC + tPA-FSN (n=5), DIC + tPA-CS-IgG (n=6)) (**E**) at the wound sites for each treatment group are shown as well as fibrinogen levels from plasma samples from control, vehicle, and all DIC groups (control (n=5), vehicle (n=6), DIC + saline (n=7), DIC + FSN (n=7), DIC + tPA-FSN (n=5), DIC + tPA-CS-IgG (n=5)) (**F**). Platelet count from blood collected is shown (control (n=6), vehicle (n=7), DIC + saline (n=7), DIC + FSN (n=8), DIC + tPA-FSN (n=5), DIC + tPA-CS-IgG (n=6)) (**G**). Clot formation from all treatment groups is shown (**H**) taken with confocal microscopy and corresponding fiber density quantification (control (n=6), vehicle (n=7), DIC + saline (n=7), DIC + FSN (n=7), DIC + tPA-FSN (n=5) DIC + tPA-CS-IgG (n=6)) with an average of 3 images per animal (**I**). A Zeiss Laser Scanning Microscope (LSM 710, Zeiss Inc., White Plains, NY, USA) was used for confocal images. 1.89 μm z-stack images were taken with objective C-Apochromat 63x 1.2W. Images were analyzed using ImageJ to make 8-bit 3D projections of z-stack images. Fiber density was quantified by determining the ratio of black (fiber) over white (background) pixels in each binary image. Data is presented as average +/- standard deviation. Data sets were analyzed via a one-way analysis of variance (ANOVA) with a Tukey's post hoc test using a 95% confidence interval. *$p<0.05$, **$p<0.01$, ***$p<0.001$, ****$p<0.0001$.

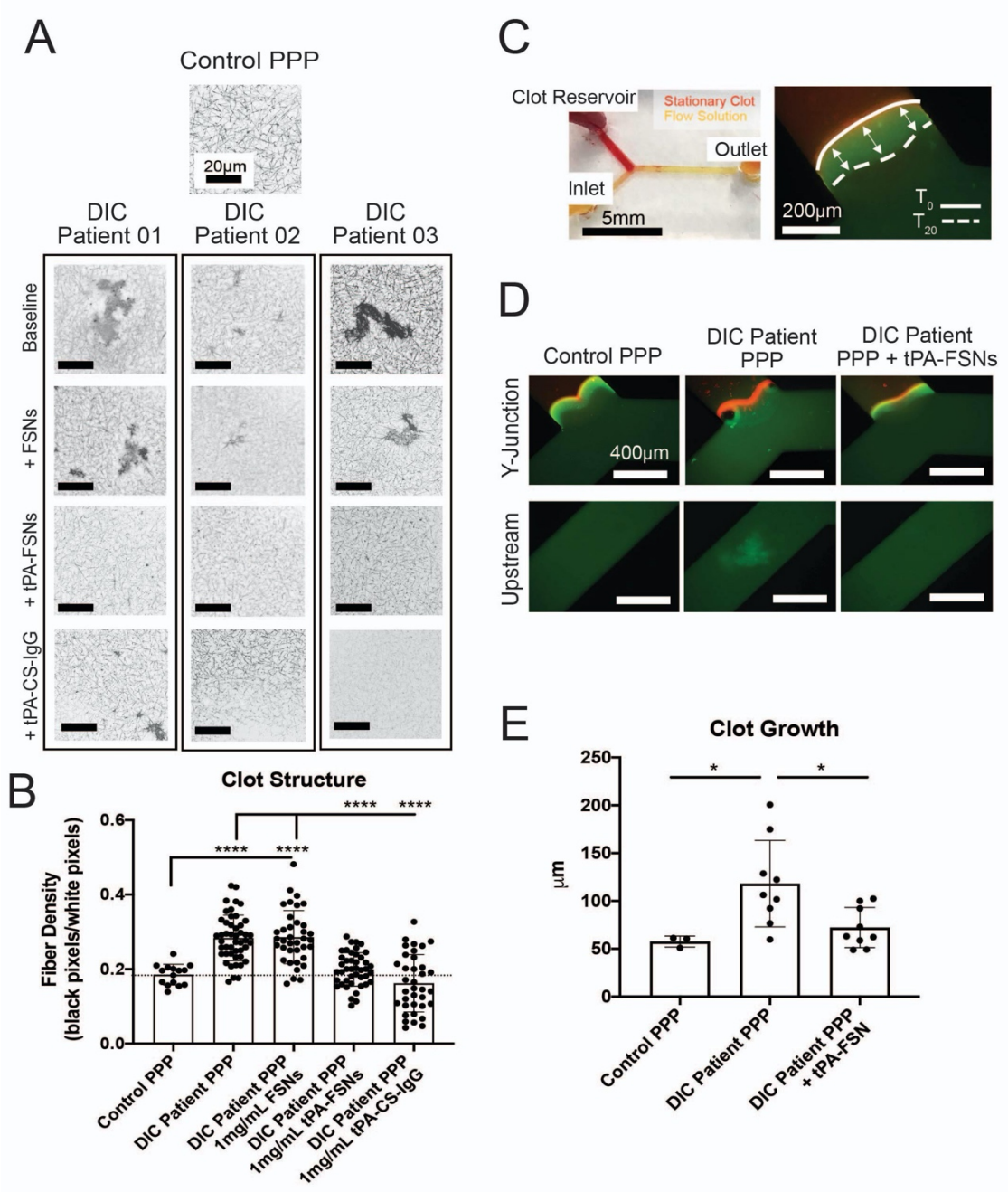

Figure 6: Effects of tPA-FSN treatment on *ex vivo* DIC patient plasma samples. Confocal microscopy images (**A**) and fiber density (**B**) quantification of DIC patient plasma clot samples compared to normal human plasma clots. A Zeiss Laser Scanning Microscope (LSM 710, Zeiss Inc., White Plains, NY, USA) was used for confocal images. 1.89 µm z-stack images were taken objective C-Apochromat 63x 1.2W. Images were analyzed using ImageJ to make 8-bit 3D

projections of z-stack images. Fiber density was quantified by determining the ratio of black (fiber) over white (background) pixels in each binary image. Unloaded FSNs, tPA-FSNs, or tPA-CS-IgG (1mg/mL) were also incorporated into DIC patient plasma clots and examined with confocal microscopy with quantified fiber density. Three DIC patient's plasma samples were examined. Pooled data from the three DIC patient samples is represented (**B**). A custom-made Y-shaped microfluidic device (**C**) tested plasma samples under flow at wall shear rate of 10 s^{-1}. A stationary fibrin clot was formed at the top Y-junction with DIC patient plasma containing Alexa-Fluor 594 labeled fibrinogen for visualization. Flow solutions contained DIC patient plasma and Alexa-Fluor 488 labeled fibrinogen for visualization. Images were taken on an EVOS FL Auto Imaging System at 10x magnification at the Y-junction and upstream inlet channel and are shown with a reference to how clot growth was measured (**C, D**). Quantification of clot growth at the stationary clot boundary (**E**) was conducted on ImageJ software. Normal healthy human plasma acted as a control. For each DIC patient's plasma sample (n=3 DIC patients), three trials were conducted with plasma alone in the flow solution, and three trials were conducted with plasma containing tPA-FSNs in the flow solution. All data is presented as average +/- standard deviation. Data sets were analyzed via a one-way analysis of variance (ANOVA) with a Tukey's post hoc test using a 95% confidence interval. *$p<0.05$, ****$p<0.0001$.